Nonstoichiometric Defects and Optical Properties in LiNbO 3

ARTICLE *in* THE JOURNAL OF PHYSICAL CHEMISTRY B · DECEMBER 2001

Impact Factor: 3.3 · DOI: 10.1021/jp004384r

ARTICLES

Nonstoichiometric Defects and Optical Properties in $LiNbO_3$

I. V. Kityk* and M. Makowska-Janusik

Institute of Physics WSP, PL-42201, Al. Armii Krajowej 13/15, Częstochowa, Poland

M. D. Fontana, M. Aillerie, and F. Abdi

Laboratoire Materiaux Optiques a Proprietes Specifiques, CLOES, University of Metz, and Supelec, 57070 Metz, Cedex, France

Received: December 6, 2000; In Final Form: May 13, 2001

The influence of intrinsic defects on optical properties of lithium niobate studied using an electronic-structure simulation technique. The simulation technique is based on molecular dynamics cluster geometry optimization, nonlocal pseudopotential calculation, and Green function electron−phonon interaction. Two models of defects are considered. The first one (electrostatically highly imbalanced) corresponds to mixture of oxygen vacancies and Nb_{Li} antisites. The second one corresponds to the Nb antisites charge compensated by appropriate vacancies, e.g., lithium vacancies, and corresponds to more realistic defect configuration. We present a band energy approach with a molecular dynamics cluster optimization that accounts for the various structural modifications related to the nonstoichiometry of $LiNbO_3$ crystals. The variation of the optical properties with the deviation from the stoichiometric composition can be understood within this approach. Especially, the role of the electron−phonon contributions to the electrooptics coefficient is shown. Comparison of the first and second models shows that the virtual model corresponding to mixture of oxygen vacancies and Nb_{Li} antisites is more suitable for describing of the optical properties. In particular, model calculations yield a large dependence of the electrooptics coefficient r_{22} on the crystal composition, in agreement with the experimental data. The observed minimum of the r_{22} coefficient versus the nonstoichiometry in the plot is interpreted as being by a diminishing in the noncentrosymmetry of the electrostatic potential around $Nb-O_6$ clusters.

1. Introduction

It is well known that the optical properties of $LiNbO_3$ (LN) single crystals are sensitive to intrinsic defects.[1−3] It was recently reported that the optical properties of pure $LiNb0_3$ (LN) crystals are sensitive to the presence of the intrinsic defects related to the nonstoichiometry of the crystals.[2] The electrooptic[1] and nonlinear optical properties[2] were shown to be strongly dependent on the concentration of these intrinsic defects. This aspect applies as well to theoretical interest. Therefore, it is of primary importance to control the real composition of the crystal, or its deviation from the stoichiometric composition.

We introduce the parameter X_c, defined as a ratio between the Li concentration and the total amount of cations (Li+Nb) to characterize the deviation from the stoichiometry. There exist various methods to determine the crystal composition X_c (ref 4). Among them, the calibration of crystals from measurements of the refractive index,[5] the absorption band edge,[6] or the Raman phonon line width.[4] However, no investigations on calculations are available that are concerned with the microscopic origin and the physical mechanisms explaining the large dependencies of linear and nonlinear optical properties on the composition X_c.

All the previous considerations of the nonlinear optical susceptibilities in congruent LN were based on a phenomenological bond length approach.[7] However, it is obvious that in the case of LN single crystals neglected by the long order crystalline band energy structure, contributions to the band energy could lead to an essential error in determining how much local rearrangements contribute to the nonlinear optical susceptibility. In the paper[1] it was shown that the stoichiometric long-range crystal interactions of pure LN crystals contribute at least 16% for pure electronic and about 9% for the phonon part. An oversimplified cluster approach to evaluate the nonlinear optical susceptibility was usually used, and the long-range contributions were calculated using renormalization of only a macroscopic dielectric susceptibility.

Such an approach could be partially suitable for an ideal (perfect) crystalline but is absolutely insufficient for doped crystalline systems. To resolve the problems mentioned above we will consider the band energy for the perfect (pure stoichiometric) crystal and then take into account existing defect states. The latter can be considered as a modulation of the ideal crystalline structure by the long-range defect fields. Two models of defects are considered. The first one (electrostatically highly imbalanced) corresponds to mixture of oxygen vacancies and Nb_{Li} antisites. The second one corresponds to Nb antisites charge compensated by appropriate vacancies, e.g., lithium vacancies, and corresponds to more realistic defect configuration. In the

10.1021/jp004384r CCC: $20.00
Published on Web 11/17/2001

present article, the first model we will indicate as a virtual defect configuration and the second one as a real defect configuration.

Based on the band energy structure calculations, we evaluate spectral dependencies of the imaginary part of the dielectric susceptibility $\epsilon_2(E)$ for various values of the parameter X_c and determine particular contributions of the different cluster groups to the optical spectra. A similar approach has been successfully used by us for the disordered materials: glasses,[8] guest−host polymers[9] complex, and doped crystals.[10] The investigated LN crystals can be considered as slightly disordered crystals. As a consequence, the mentioned approach may be used. We have revealed that for an explanation of optical spectra and especially nonlinear optical properties, a better agreement has been achieved using a norm-conserving pseudopotential (NCPP) method because the optical effects are determined first of all by the external valence electrons and unoccupied excited states. Unfortunately, self-consistent eigenenergy convergence within a framework of the one-electron band energy calculations is not sufficiently for performing the molecular dynamics geometry optimization. Therefore, an additional molecular dynamics procedure is necessary. As the external electrostatic field we used one-electron band energy solid-state calculations.[11] In the case of the second-order nonlinear optical effects (particularly, of the optical second harmonic generation), contrary to the usual optical effects, the noncentrosymmetry in the charge density distribution plays a key role.[12] Therefore, appropriate connection of the solid-state approach with the local structure optimization will be applied. Moreover, in the case of the linear electrooptics, substantial contribution gives phonon subsystems. All the consideration will be done both for the real as well for the virtual defect configuration.

The main principles of our approach are the following: (a) band energy structure calculations of the LN using the ab initio norm conserving pseudopotential method for the pure and nonstoichiometric specimens; (b) determination of the optical constants depending on the degree of nonstoichiometry; (c) calculations of the $[Nb-O_6]$ cluster charge density distribution with and without taking into account the molecular dynamics simulations and optimization of the cluster geometry and with taking into account a redistribution of the electrostatic potential space distribution within the clusters; (d) simulation of the electrooptic coefficients behavior depending on the nonstoichiometry, taking into account the electron and phonon subsystems.

Band energy structure for the LN crystals with different X_c is presented in section 2. Molecular dynamics procedure and the geometry optimization is reported in section 3. Structural rearrangements of particular clusters are presented depending on the X_c. Section 4 presents the phonon contributions to the electrooptic coefficient r_{22} calculated for the crystals with various stoichiometry. Particular contributions of the UV− electronic states modified by effective electron−phonon interactions are presented in the section 5. A discussion concerning agreements and discrepancies between the proposed approach and experimental data is carried out.

2. Electronic Structure of LN Crystals with Intrinsic Defects

A more appropriate method of band energy structure calculations for the kinds of systems discussed here seems to be the NCPP calculation method.[13] This method concerns the optical data. The NCPP method has been successfully applied for simulation of the optical spectra in the different crystalline as well noncrystalline systems[14] having intrinsic and extrinsic defects.

We perform a detailed calculation of the band electronic structure and of the appropriate optical properties of the LN crystals using the first-principles NCPP method in the local approximation of density-functional theory. This method has also been successful in the calculation of the nonlinear optical properties of complex systems,[15] metallic glass systems,[8] polymer-like systems,[9] etc. The LN crystals with different nonstoichiometry can be considered as slightly disordered systems. Therefore, applying the NCPP method to the mentioned systems seems to be reasonable.

The total energy functional was expressed within a framework of the local density functional approach and of a Hartree−Fock minimization procedure and was carried out toward the charge density $\rho(r)$:

$$E_{tot}[\rho(r)] = T[\rho(r)] + V_{n-e}[\rho(r)] + V_{e-e}[\rho(r)] + V_{e-c}[\rho(r)] \quad (1)$$

where

$$\rho(r) = \Sigma\Sigma_{\beta,1}|\Psi(l,\mathbf{r},\beta)|^2 \quad (2)$$

The kinetic energy functional $T[\rho(r)]$ is a functional of charge density; $V_{n-e}[\rho(r)]$ corresponds to nuclear-electron Coulomb-like interaction that, in the present case, is chosen in the form described in ref 14. A nonlinear extrapolation procedure was conducted to evaluate the corresponding NCPP in the form convenient for the analytical evaluations (Gaussian-polynomial-like), particularly:

$$V_{n-e}^{(\beta,l)}(r) = \Sigma_i(A_i^{\beta} + r^2 A_{i+3}^{\beta}) \exp(-\alpha_n^{(l,\beta)} r^2) \quad (3)$$

where β determines a kind of atom; l is an appropriate angular momentum, and the value of n depends on the precision of the fitting procedure for the corresponding nonlinear interpolation procedure and is varied between 1 and 5. During the nonlinear interpolations, NCPP has been expressed in the form of at least 18 Gaussian-polynomial terms with decaying exponents in the range 0.001−835000. The basic wave functions consisted of 1s-5d orbitals of Nb, 1s-3p orbitals of Li, and 1s-4s orbitals of O. We have included excited orbitals in order to enhance precision of the matrix dipole momentum values, especially for optical properties simulation. The proposed approach allows to achieve the eigenvalue convergence up to 0.0013 eV. $V_{e-e}[\rho(r)]$ and $V_{e-c}[\rho(r)]$ are screening potentials corresponding to electron−electron and exchange-correlation interactions, respectively. Coefficients A and α are evaluated fitted coefficients determined by the nonlinear extrapolating procedure.

The proposed form of the NCPP allows to obtain the corresponding matrix elements in an analytical form. The procedure involves resolving the following secular equation:

$$||[h^2(k + G_{n,n'})^2/2m - E(\mathbf{k})]\delta_{n,n'} + \Sigma\Sigma_{\alpha}V_{\alpha}(\mathbf{G}_n' - \mathbf{G}_n)S_{\alpha}(\mathbf{G}_n' - \mathbf{G}_n)|| = 0 \quad (4)$$

where $E(\mathbf{k})$ is the searched eigenenergy for a given $\mathbf{k}$ point of the BZ; $\mathbf{G}_n'$ and $\mathbf{G}_n$ are interacting basis plane waves. For the stoichiometry specimens, we have taken into account at least 3680 plane waves, and additional 1244 plane waves were taken in the Lowdin perturbation approximation. The stability of the eigenenergy, within the 0.0015 eV, was chosen as a criterion of the convergence. For the nonstoichiometric cases, we have taken into account at least 4286 and 1346 plane waves, respectively. We have found that an increase of the convergence limit from 0.02 eV to 0.002 eV causes maximal shift of the

particular energy bands less than 0.04 eV that correspond to the changes of the matrix dipole moments less than 8.2%.

Resolution of the mentioned secular equations was carried out using the QL-modified Jacobi method. The structural factor for the β type atom was evaluated in the form

$$S_{\beta}^{(\alpha)}(\mathbf{G}_n' - \mathbf{G}_n) = g^{(\alpha)}/N\Omega\Sigma\beta \exp[-i(\mathbf{G}_n' - \mathbf{G}_n)\,\tau_{\beta}] \quad (5)$$

Here, $g^{(\alpha)}$ corresponds to the particular contributions of the αth ions and is given by the stoichiometry X_c. Varying the weighting coefficients of $g^{(\alpha)}$ we obtained the band energy structures for the given nonstoichiometry. The Fourier transformations of the pseudopotential for the αth type of ions take the form

$$V_{\alpha}^{(\alpha)}(\mathbf{G}_n' - \mathbf{G}_n) = 1/\Omega \int V^{(\alpha)}(\mathbf{r}) \exp[-i(\mathbf{G}_n' - \mathbf{G}_n)\mathbf{r}]\, d^3\mathbf{r} \quad (6)$$

Electron screening effects were calculated using parameterized Perdew−Zunger[16] and Ceperley-Alder expressions.[17]

A special method of Chadhi-Cohen[18] was used for calculation of the space electron charge density distribution. The latter was used to construct the charge density functional of electrons. The diagonalization procedure was performed in the 32 special points of the Brillouin zone (BZ), and afterward an extrapolation was done using a perturbation **kp** method.

Acceleration of the iteration convergence was done by mixing the $(m-1)$th iteration with 70% of the output ρ before substitution into the next equation. A criterion of the self-consistency was satisfied after ensuring the condition

$$|\rho_{\text{out,m}} - \rho_{m\text{np,m}}| < \epsilon \quad (7)$$

after the mth iteration step. We assumed an accuracy less than $\epsilon = 8.5\%$ between the input and output iterations as a main criterion of the self-consistence. The energy eigenvalues were stable within a range of 0.002 eV. The numerical evaluations of the charge density functional terms were carried out using a numerical tetrahedral method.

We started the calculations for the perfect stoichiometric crystals with the factor $g^{(\alpha)}$ equal to 1. Afterward, the factors $g^{(\alpha)}$ were varied appropriately to the given X_c. All of the calculations were performed for the 412 points of the BZ. The general form of the band energy dispersion was in agreement with that obtained in ref 19. It is interesting that independent of the type of local cluster chosen, dispersion of the energy bands in the **k**-space is only sensitive to variation of X_c. This will be a subject of a separate work.

Comparing the calculated bands with the experimental data of the X-ray photoelectron spectroscopy,[20] we revealed an agreement up to 0.17 eV. The value of the calculated energy gap was less than 3.69 eV, compared with the 3.80 eV obtained from the absorption edge. The refractive index was equal to 2.1578, which is very close to the experimentally measured value of 2.1397.[1] All these data show that the adopted approach is sufficient for explaining of the main optical parameters. We have found that maximal deviation from the perfect band structure is observed for $X_c = 48.4\%$. On the basis of the performed band energy calculations, we performed evaluations of the imaginary part of the dielectric susceptibility using the equation

$$\epsilon_2(E) = 2\pi N\, e^2/h^3 \sum_{v,b,\mathbf{k}} \int |\langle \Psi_{v,b}(\mathbf{k},\mathbf{r}) | \vec{\nabla}\vec{\mathbf{r}}\, \Psi_{c,b}(\mathbf{k},\mathbf{r}) | \rangle\, d^3\mathbf{r}\, \delta(E_{v,b}(\mathbf{k}) - E_{c,b}(\mathbf{k}) - E) \quad (8)$$

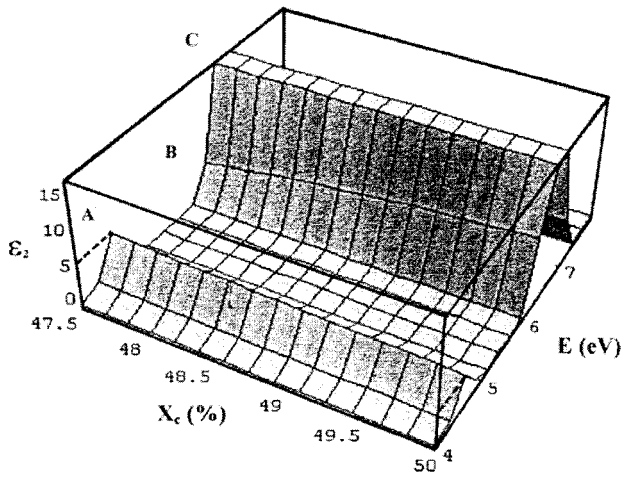

Figure 1. Imaginary part of the dielectric susceptibility ϵ_2 versus the energy E with various compositions X_C.

where $\Psi_{v,b}(\mathbf{k},\mathbf{r})$ and $\Psi_{c,b}(\mathbf{k},\mathbf{r})$ correspond to the valence and conduction band pseudo wave functions, respectively. All of the summation is performed over the whole Brillouin zone.

In Figure 1 is reported the spectral dependence of the imaginary part of the dielectric susceptibility $\epsilon_2(E)$ for crystals with various compositions, as calculated by the methods described above. It is necessary to underline that the calculated behavior was independent of the type of local defect configuration and was in good agreement with experimental data.

The changes in the energies are more clear for the bands (indicated by B and C) originating prevailingly from the 2p O orbitals. This once more confirms that the main changes of the band's electron structure originating from the delocalized oxygen states. The 4d Nb states (indicated by the letter A in Figure 1) forming the conducting band states are less dependent on X_c. Core-like 2s O bands are independent of X_c.

First of all, we should point out an apparent anisotropy of energy dispersion with decreasing X_c. This is caused by anisotropy in the localization of the corresponding band carriers. The presented data unambiguously indicate that the nonstoichiometry essentially influences the density of states and the carrier effective mass determining the band electron localization. The increase of the carrier localization was revealed for $X_c = 48.4\%$. For $X_c = 49.5\%$, this localization drastically decreased. For $X_c = 49.5\%$, the localization is maximally similar to the perfect LN crystals. More prominently, this dependence is presented in the three-dimensional Figure 1. Such complicated dependencies of the band energy localization reflect a competition between the long-range crystalline ordering in the perfect crystals and local disorder due to the presence of an oxygen defect. The maximal deviations compared with the perfect crystals in the band energy dispersion are as much as 0.22 eV, but the performed minimization procedure within the framework of the one-electron approach is not satisfactory enough for the total energy minimization within the particular structural clusters. Similarly, as in the case of the disordered materials[9] in the nonstoichiometric LN crystals, we should do additional molecular dynamics simulations within the particular clusters in order to explain the observed changes of the noncentrosymmetry and of the corresponding electrooptic coefficients described by the third-order polar tensors.

The nonlinear increase of the oscillator B can be related to oxygen-vacancy disturbed states, since the concentration of the oxygen vacancy decreases as X_c rises simultaneously with

increasing Li site occupation by Li ions. It can be mentioned that our calculations (decrease of the peak A) are in agreement with the experimental shift of the energy gap with X_c.

The calculations performed by us have shown that an increase of the convergence limit from 0.02 eV to 0.00042 eV changes the appropriate dipole momenta less than 9%. Therefore, to evaluate the observed changes of the optical constants (not the values) in electrooptics behavior versus stoichiometry, it is sufficient to carry out the simulations with the convergence limit within the range 0.02 to 0.002 eV.

The results presented above indicate that, even without the molecular dynamics, structural rearrangement near the defect can explain the main linear optical effects (absorption, refractive index, etc.) as well the band energy width (X-ray photoelectron spectroscopy). However, this approach is not enough to explain the nonlinear optical properties, particularly of the electrooptic effects. This problem will be considered in the next section. We have checked also that contributions of the energy oscillators with energies higher than 7.5 eV create only an effective background that is nonsensitive to the nonstoichiometry. Spectral behaviors are coincident for the mentioned two models of defects.

3. Molecular Dynamics Simulations

In section 2 we have proven that the band energy calculations show nonmonotonic behaviors versus X_c for the main optical oscillators, even if the local structural rearrangement due to the presence of the intrinsic defects may be neglected. In the present section we will show how the band energy contributions disturb the local clusters NbO_6 or LiO_6. For this reason, we use ab initio molecular dynamics geometry optimization.

As a starting point we have used a hybrid Becke's method[21] using the elecrostatic potential parameters obtained from the ab initio band energy structure calculations. The main advantage of this method is that it consists of a very fast convergence of the eigenvalues with respect to the size of the basis sets. Geometry optimization for each crystal composition was done using the gradient-corrected potential functional in the electrostatic potentials with the step of 0.05%, and the harmonic frequencies for subsequent calculations were determined by an analytical differentiation of the Hessian matrices.

The nondynamic correlation was taken into account within the molecular cluster self-consistent functional approach included in the GAMESS program.[22] Geometry optimizations were performed using the gradient conditions of the GAMESS program, and the dynamics boundary conditions have been applied. Afterward we calculated the matrix dipole moments. The equilibrium atom positions were obtained from a condition for the minimum of the total energy U_{tot}.

We have found that the picture around the NbO_6 clusters is strongly dependent on the crystal composition, whereas the electrostatic potential around the LiO_6 cluster was nearly insensitive to a change of X_c. Therefore, only the [Nb−O_6] clusters will be considered. Moreover, it is well known from simpler approaches that these clusters play a key role in the observed effects.

From Figure 2 one can see a redistribution of effective electrostatic potentials depending on the nonstochiometric X_c obtained after and before the performed molecular dynamics geometry optimization. For convenience, one can see a shift of the effective center position of the electrostatic potentials from equilibrium positions. One can see that for $X_c = 48.7\%$ the distribution of the electrostatic potential in the *XY* crystallographic plane is more centrosymmetric than when comparing the two other cases. Parameters of the cation−anion distances within the [Nb−O_6] cluster are presented in Table 1 for more clarification. The presented data unambiguously show that the performed molecular dynamics geometry optimizations cause additional structural stabilization (lowering of the total energy U_{tot}). More interesting is the fact that the distances between Nb−O(1) and Nb−O(2) correlate well with the apparent noncentrosymmetry. Comparing Figure 2 and the data in Table 1, one can unambiguously see the essential role of the additional geometry optimization for obtaining the more stable geometry structure (lower total energy) and appearance of the noncentrosymmetry in the electrostatic potential distribution.

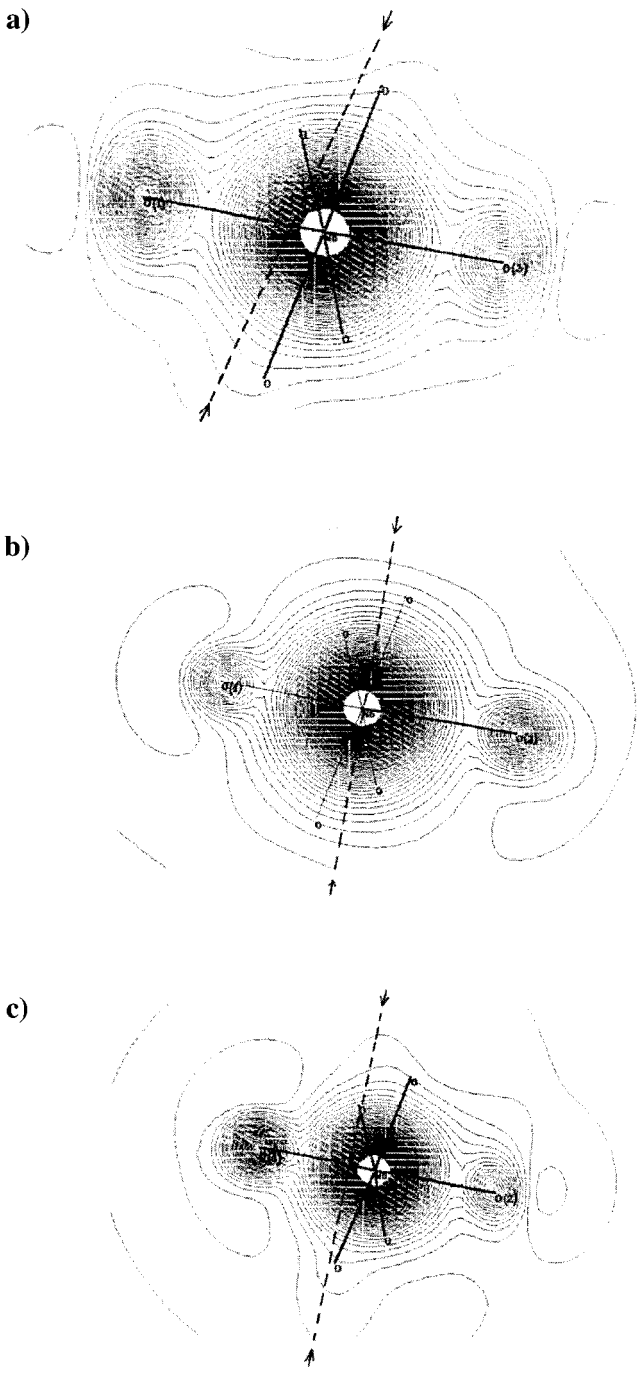

Figure 2. Electrostatic potential distribution around [Nb−O_6] clusters for different X_c: (a) 48.4%; (b) 49.1%; (c) 49.9%.

TABLE 1: Main Distances between the Main Ions within the [Nb−O_6] before and after the Molecular Dynamics Geometry OptimizAtion Procedure for the Virtual Defect Configuration[a]

N	before molecular dynamics simulation			after molecular dynamics simulation		
X_c, %	Nb−O(1), A	Nb−O(2), A	U_{tot}, eV	Nb−O(1), A	Nb−O(2), A	U_{tot}, eV
48.4	2.321(8)	2.304(7)	−22.12(0.02)	2.333 (0.012)	2.269(0.012)	−26.94(0.02)
				2.328	**2.278**	**−22.57**
48.7	2.313(3)	2.294(4)	−19.68(0.02)	2.304(0.012)	2.261(0.012)	−25.75(0.02)
				2.301	**2.257**	**−21.46**
49.5	2.302(1)	2.292(5)	−24.35(0.02)	2.319(0.012)	2.280(0.012)	−27.35(0.02)
				2.314	**2.287**	**−24.56**

[a] Bold entries indicate data for the real defect configuration.

Table 1 confirms the conclusion obtained for the disordered materials concerning the necessity of additional total energy optimization within the particular structural clusters. Particularly interesting are the data indicating that the real defect configuration leads to a substantial redistribution of the local charge density distribution and that, for the real defect states, total energy per atom is higher.

4. Phonon Contributions to the Electrooptic Coefficients

It is well known that taking into account the phonon states plays an important role in the calculation of electrooptic coefficients. Therefore, in this section we will attempt to evaluate the particular contributions of the phonon modes to the calculated electrooptic coefficient r_{22}. Such an approach was successfully developed for chalcogenide glasses and is here extended to the slightly disordered crystals (nonstoichiometric LN).

The quantum chemistry calculations were performed self-consistently after separation of the electron and phonon contributions. The Schroedinger equation for pure phonons was expressed within an harmonic approximation:

$$d^2\Psi_k/dQ_k^2 + [8\pi^2\mu_k h^{-2}\Omega_k - 4\pi^2\mu_k h^{-2}\Omega_k^2]\Psi_k = 0 \quad (9)$$

where Ψ_k is a wave function corresponding to kth normal coordinate Q_k; μ_k denotes a reduced mass of the nuclei taking part in the kth phonon mode. It is obvious that solutions to the above equation are determined by a model that is responsible for the force constant calculations (so-called Hessian matrices), i.e., the second derivatives of an electrostatic cluster potential with respect to given normal coordinates. All the phonon frequencies have been fitted to the experimental Raman data.[4]

In addition to the usual harmonic modes, we have taken into account also the electron−phonon interaction potential that was calculated in a nonlinear approximation[22]:

$$V_{e-ph}(\mathbf{r}_i) = e^2\sum_{ms} M_{ms}^{-1/2}[Z_{ms}(\mathbf{r}_s - \mathbf{u}_{ms})|\mathbf{r}_s - \mathbf{u}_{ms}|^{-3} - \sum_{m's'} Z_{m's'}(\mathbf{r}_{s'} - \mathbf{u}_{m's'})|\mathbf{r}_{s'} - \mathbf{u}_{m's'}|^{-3}] \quad (10)$$

where M_{ms} and eZ_{ms} are the effective ionic mass and charge; the corresponding ions are labeled by m and s, respectively. The $\mathbf{u}_{ms,m's'}$ vector is a relative displacement of two ions from their equilibrium positions $\mathbf{r}_s$ and $\mathbf{r}_{s'}$. The probability of a one-phonon transition induced by the vibration of a frequency Ω_k is equal to

$$W(\Omega_k) = 4(h/2\pi)^{-2}c^{-3}H^{-1}g^{-1}(\mathbf{r}_i)(E_{el} - \Omega_k)^2 B(\Omega_k) \quad (11)$$

H is a sum of the η and ξ level widths, E_{el} is an energy of the interband transitions, Ω_k denotes a kth phonon energy, and $g(r_i)$ is a degeneration degree of the corresponding electron energy levels. The parameter $B(\Omega_k)$ is equal to[8]

$$B(\Omega_k) = \sum_\eta^{g(\eta)}\sum_\xi^{g(\xi)} |\{\sum_\varphi \langle\eta,\eta_\Omega|V_{e-ph}(\mathbf{r}_i)|\varphi,\eta_\Omega+1\rangle \times \langle\varphi|\mathbf{d}|\xi\rangle (E_\xi - E_\eta + \Omega_k)^{-1} + \sum_\varphi \langle\eta|\mathbf{d}|\varphi\rangle \times \langle\varphi,\eta_\Omega|V_{e-ph}(\mathbf{r}_i)|\xi,\eta_\Omega - 1\rangle (E_\xi - E_\eta - \Omega_k)^{-1}\}|^2_\theta \quad (12)$$

where the η and the ξ are the lower and upper electron MO energy levels, respectively, φ denotes a virtual intermediate band state and $\mathbf{d}$ is an electric dipole moment for a given optical transition. The summation is performed over all degenerated initial and final states. The notation θ denotes an averaging with respect to occupation numbers of the quasiphonon states.

Our calculations have shown that the dominant role in the corresponding electrooptics coefficients belongs to the Li−O clusters because they give higher frequency resonance and are more sensitive to the disturbances caused by the Nb antisite oxygen vacancies. But we consider also the [Nb−O_6] clusters and the intercluster bridges in the first perturbation approach.

On the other hand, the phonons included in the electron−phonon interaction (eq 12) can lead to the following normal coordinates:

$$B(\Omega_k) = C_{\eta\xi}^{\gamma}(r_\lambda^\Delta)C_{\eta\xi}^{\gamma'}(r_{\lambda'}^{\Delta'})\ \mathrm{Im}\ G_{\Delta\Delta'}^{\gamma\gamma'}(r_\lambda^\Delta, \Omega_k^2) \quad (13)$$

where $G_{\Delta\Delta'}^{\gamma\gamma'}(r_\lambda^\Delta)$ is a Green function (γ and γ' are numbers of coordination sphere) defined as

$$G_{\Delta\Delta'}^{\gamma\gamma'}(r_\lambda^\Delta) = \sum_\varphi\{\langle\eta|V_{e-ph}(\mathbf{r}_i)|\varphi\rangle\langle\varphi|\mathbf{d}|\xi\rangle + \langle\eta|\mathbf{d}|\varphi\rangle\langle\varphi|V_{e-ph}(\mathbf{r}_i)|\xi\rangle\}(E_\xi - E_\eta)^{-1} \quad (14)$$

The resulting expression is given below:

$$G_{\Delta\Delta'}^{\gamma\gamma'}(r_\lambda^\Delta, \Omega_k^2) = \sum_\Omega K_{\Delta'}^{\gamma'}(r_\lambda^\Delta) K_\Delta^\gamma(r_\lambda^\Delta)(\Omega_k^2 - \Omega^2 - i\delta)^{-1} \quad (15)$$

where the coordinates $K_\Delta^\gamma(r_\lambda^\Delta)$ are obtained for a given phonon mode from averaging the electron states. To include the local lattice deformations into the Green function, we have taken into account also the [Li−O] deformation localization that allows to use the Dyson relations. The deformation potential and corresponding oxygen-vacancy charge defect disturbance determine the potential operator U and

$$G_{\Delta\Delta'}^{\gamma\gamma'}(1) = G_{\Delta\Delta'}^{\gamma\gamma'}(0) + G_{\Delta\Delta'}^{\gamma\gamma'}(0)\ U\ G_{\Delta\Delta'}^{\gamma\gamma'}(1) \quad (16)$$

where $G_{\Delta\Delta'}^{\gamma\gamma'}(0)$ and $G_{\Delta\Delta'}^{\gamma\gamma'}(1)$ are the Green functions for ideal systems and systems with defects, respectively.

The relation between real and imaginary parts of the Green function were evaluated using Kramers−Kronig dispersion

relations. The main phonon contributions come from modes with relatively high frequency originating from the [Li−O] intracluster bonds. All the phonon modes were renormalized by electron−phonon nonlinearities described above.

The contribution of the phonons to the electrooptic coefficients was calculated using the general following expression:

$$r_{ijk}^{(\omega,\omega)} = \frac{1}{\hbar^2}\frac{e^3 N}{2!}\hat{P}_{ijk}\sum_k\sum_{A,B}\left[\frac{\langle 0|i|A\rangle\langle A|j|B\rangle\langle B|k|0\rangle}{(\omega+\Omega_\alpha)(\omega+\Omega_\beta)} + \frac{\langle 0|j|A\rangle\langle A|i|B\rangle\langle B|k|0\rangle}{(\Omega_\alpha-2\omega)(\Omega_\beta-\omega)} + \frac{\langle 0|j|A\rangle\langle A|k|B\rangle\langle B|i|0\rangle}{(\omega+\Omega_\beta)(\Omega_\alpha-\omega)}\right] \quad (17)$$

where $\Omega_{\alpha,\beta}$ are eigen-frequency phonon modes; $\langle A|i|B\rangle$ are phonon mode dipole matrix elements disturbed by the electron−phonon interactions to calculate the particular EO coefficient r_{22};we let $i = j = k = 2$ in eq 17. We have performed all calculations for the Γ point of the BZ. All of the phonon modes taken into account agree with the experimetal results given in ref 4. The presented calculations allow to detect changes in the electrooptic coefficients up to 0.2 pm/V. Because the main goal of the present work consists of the simulation of the changes of the r_{22} versus the nonstoichiometry, in the chosen model the approach should be absolutely sufficient to determine the corresponding changes. The determination of the absolute values of the electrooptics coefficients is not a goal of the present work and will be a subject of a separate future work.

The calculations of the r_{22} were carried out separately for the harmonic phonon modes. Then we have superimposed phonon modes renormalized by the electron−phonon interactions. The contributions of each phonon mode to calculated electrooptic coefficient r_{22} were determined for crystals with various compositions X_c. The corresponding results are presented in Figure 3a and Figure 3b for virtual and real defect models, respectively.

For the virtual model, one can see the opposite signs of the particular phonon mode contributions to the electrooptic coefficient r_{22}. Most of the active phonon modes have positive sign contributions, whereas modes higher than 580 cm^{-1} give essentially opposite negative contributions that drastically increase with the parameter X_c This proves that the Li−O dipole plays a key role in the large value of the EO coefficient r_{22} obtained in the stoichiometric crystal. The physical origin of the opposite sign contributions can be attributed to different directions of the noncentrosymmetry within the Nb−O and Li−O shells.

For the real model, the corresponding behavior is quite different and contribution to the electrooptics versus the X_c and phonon frequency is substantially different.

5. Influence of Intrinsic Nonstoichiometry on a Dispersion of the Electrooptic Coefficients

The calculations of the electronic part of the electrooptic tensors have been carried out using the expression and the calculation techniques similar to the works[9]

$$\chi_{ijk}^{(\omega,\omega)} = \frac{1}{\hbar^2}\frac{e^3 N}{2!}\hat{P}_{ijk}\sum_k\sum_{\alpha,\beta}\left[\frac{\langle 0|i|\alpha\rangle\langle\alpha|j|\beta\rangle\langle\beta|k|0\rangle}{(2\omega+\omega_\alpha)(\omega+\omega_\beta)} + \frac{\langle 0|j|\alpha\rangle\langle\alpha|i|\beta\rangle\langle\beta|k|0\rangle}{(\omega_\alpha-2\omega)(\omega_\beta-\omega)} + \frac{\langle 0|j|\alpha\rangle\langle\alpha|k|\beta\rangle\langle\beta|i|0\rangle}{(\omega+\omega_\beta)(\omega_\alpha-\omega)}\right] \quad (18)$$

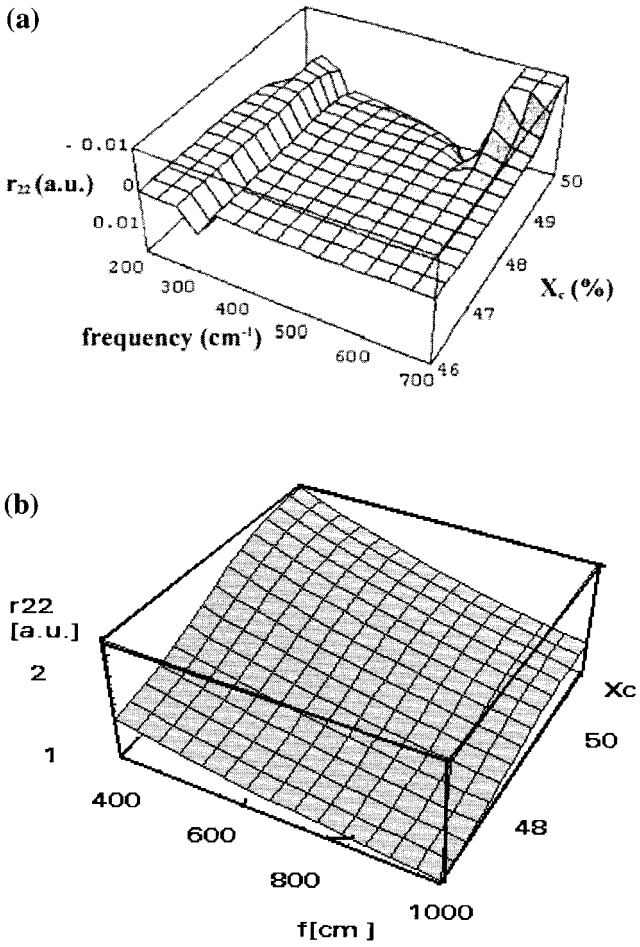

Figure 3. Ionic (phonon) contribution to the electrooptic coefficient r_{22} for different defect models: (a) virtual; (b) real.

where the $\langle\alpha|y|\beta\rangle$ are dipole matrix momenta between the α and β electronic band states; $\hat{P}$ is a permutation operator; N is the concentration of the valence electrons; the summation over the **k** means summation over the whole effective Brillouin zone. Moreover, using this expression we have evaluated also the photoinduced changes of the refractive index (photorefractive effect).

Because photoinduced birefringence is more sensitive to the changes of the vacancy occupation, we have done the simulations of the photorefraction effects and the corresponding dependences are presented in Figure 4a,b. One can see that relative changes of the refractive indices are substantially different within the two defect configuration models due to the different electron−phonon contributions. As a main criterion of validity of the model one can consider degree of agreement between experiment and theory. From Figure 4c, one can clearly see that virtual model gives substantially better agreement with experimental data than does the real defect model.

Comparing the experimental data with the theoretically calculated data, one can see good agreement. It is necessary once more to underline that the developed approach is valuable for simulation of the changes of the electrooptic coefficients versus the nonstoichiometry parameters. However, to determine the absolute values of the electrooptic coefficients the precision of the dipole moments should be enhanced. Moreover, the experiment concerning determination of the absolute r_{22} electrooptic coefficient is not always sufficient for comparison with theory. At the same time, the changes give more important

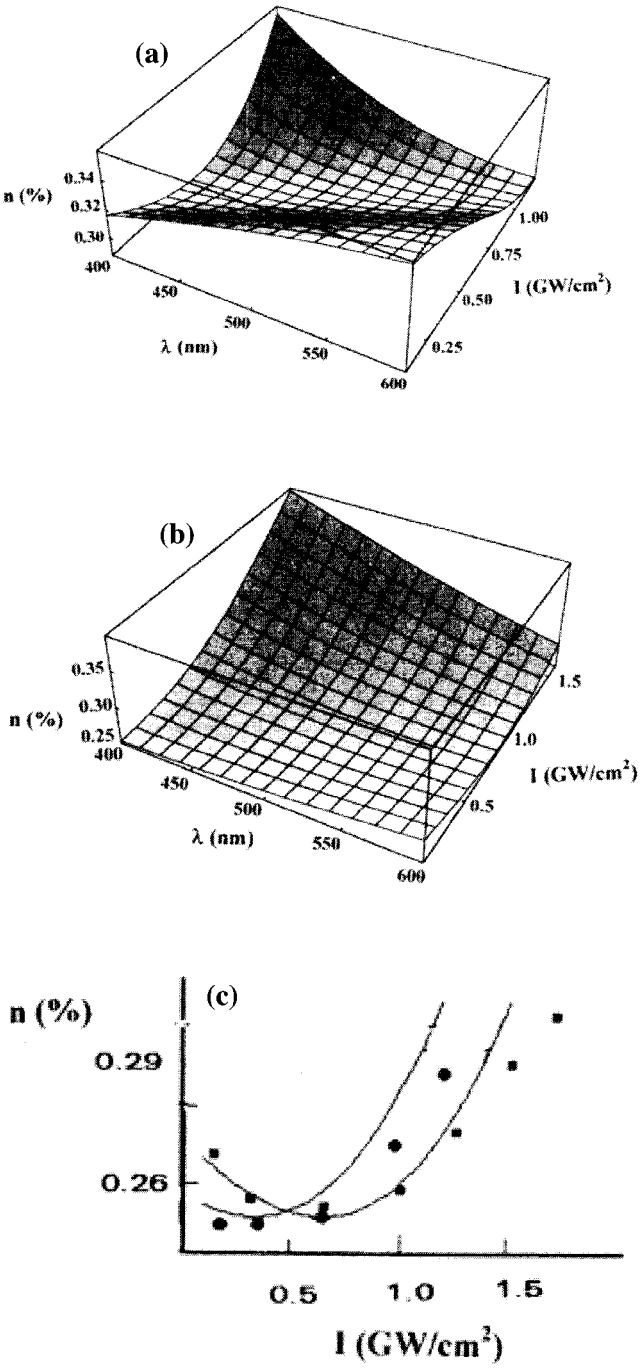

Figure 4. Relative changes of spectral dependences of refractive indices under influence of the photoinduced nitrogen laser beam intensity *I*: (a) virtual defect model; (b) real defect model; (c) comparison of the experimental behavior with the theoretical curves (●) $\lambda = 420$ nm; (■) $\lambda = 500$ nm.

information for the technologist showing the main directions of the electrooptic r_{22} coefficient changes.

Conclusions

Two defect configurations were considered: The first one (electrostatically highly imbalanced) corresponds to mixture of oxygen vacancies and Nb_{Li} antisites. The second one corresponds to Nb antisite charge compensated by appropriate vacancies, (e.g., lithium vacancies) and corresponds to more realistic defect configuration. We have revealed that the linear optical properties are insensitive to the chosen defect configurations. However, photorefraction and electrooptic effects show substantial sensitivity to the chosen model. Our investigations have shown that the virtual electrostatically imbalanced model gives better agreement with experiment comparing with the real model.

An essential influence of near-the-defect oxygen on the noncentrosymmetry of the electrostatic potential is shown. The electronic part of the [Nb−O] clusters gives more than 50% to the total output electrooptic coefficient r_{22}. The phonon subsystem essentially increases its contribution to r_{22} within the $X_c = 48.4-48.8\%$ range, causing several disturbances of the long-range translations.

References and Notes

(1) Abdi, F.; Aillerie, M.; Bourson, P.; Fontana, M. D.; Polgar, K. *J. Appl. Phys*. **1998**, *84*, 2251.

(2) Schlarb, U.; Betzler, K. *Phys. Rev. B* **1993**, *48*, 15613.

(3) Schlarb, U.; Betzler, K. *Phys. Rev. B* **1994**, 50, 751.

(4) Ridah, A.; Bourson, P.; Fontana, M. D.; Malovichko, G. *J. Phys.: Condens. Matte*r **1997**, *9*, 9697.

(5) Wohleke, M.; Corradi, G.; Betzler, K. *Appl. Phys. B* **1996**, *63*, 323.

(6) Kovacs, L.; Ruuschhaupt, G.; Polgar, K.; Corradi, C.; Wohleke, M. *Appl. Phys. Lett*. **1997**, *70*, 2801.

(7) Donnenberg, H. *Atomic Simulation of Electrooptic and Magnetooptic Oxide Materials*; University of Osnaabruck, Springer-Verlag: Berlin, 1999; 33.

(8) Kityk, I. V.; Sahraoui, B. *Phys. Rev. B* **1999**, *60*, 494. Kityk, I. V.; Jakubczyk, E. *Appl. Optics* **1999**, *38*, 5162.

(9) Kityk, I. V.; Sahraoui, B.; Nguyen, P. X.; Rivoire, G.; Kasperczyk, J. *Nonlinear Optics* **1997**, *18*, 13.

(10) Malachowski, M.; Kityk, I. R.; Sahraoui, B. *Phys. Status Solidi* **1998**, *207*, 405.

(11) Kityk, I. V.; Yaszczishin, I. N.; Tyagnyriadko, L. V. *Glass Phys. Chem.* **1994**, *20*, 404.

(12) Golis, E.; Kityk, I. V.; Kasperczyk, J.; Wasylak, J. *Mater. Res. Bull.* **1996**, *9*, 1057.

(13) Bachelet, G. B.; Hamann, D. R.; Schluter, M. *Phys. Rev. B* **1982**, *26*, 4199.

(14) Kolinko, M. I. *Phys. Rev. B* **1997**, *55*, 5007.

(15) Kityk I. V. *Phys. Solid State* **1991**, *33*, 1026.

(16) Perdew, J. B.; Zunger, A. *Phys. Rev. B* **1981**, *23*, 5048.

(17) Ceperley, D. M.; Adler, B. J. *Phys. Rev. Lett*. **1980**, *45*, 161.

(18) Chadhi, D. J.; Cohen, M. L. *Phys. Rev. B* **1973**, *8*, 5747.

(19) Ching, W.-Y.; Gu, Z.-Q.; Xu, Y.-N. *Phys. Rev. B* **1994**, *50*, 1992.

(20) Kityk, I. V. *Ukr. Phys. J*. **1990**, *32*, 678.

(21) Becke, A. D. *J. Chem. Phys*. **1994**, *98*, 1372 and 5648.

(22) GAMESS, Package of the computer programms, 1997, 235 p.